RAPID COMMUNICATIONS

PHYSICAL REVIEW A VOLUME 48, NUMBER 5 NOVEMBER 1993

Quantum calculations for one-dimensional laser cooling: Temporal evolution

T. Bergeman

Department of Physics, State University of New York at Stony Brook, Stony Brook, New York 11794-3800

(Received 13 May 1993; revised manuscript received 29 July 1993)

Calculations of the temporal evolution of the fully quantal density matrix for laser cooling of atoms show features not present in steady-state results. For polarization gradient cooling, the average kinetic energy in the cold-atom peak after 1000 radiative lifetimes decreases with increasing F_g, and is <1 recoil energy at low laser intensity. With magnetically induced laser cooling (MILC) and low optical pumping rates, atoms cool slowly within the potential wells, giving minima in the velocity distribution at $v = 0$. MILC is seen as a cyclic process; optical pumping cools and B-field mixing slightly heats.

PACS number(s): 32.80.Pj, 42.50.Vk

In view of many recent advances in techniques for cooling atoms by laser light, there is interest in theoretical methods that can address diverse experimental situations. Most of the theoretical results presented to date have been for the steady-state limit of the cooling process. For example, semiclassical theories [1,2] for atom cooling employ a force versus velocity function and a diffusion parameter based on the steady-state solution of the density-matrix equations. The first examples of density-matrix calculations with a basis of quantized translational states [3,4] also presented steady-state solutions, obtained by inverting the evolution matrix. Also, except for one notable discussion of Doppler cooling [5], reports to date on quantum Monte Carlo calculations [6–9], which have been successful in a variety of applications, have focused primarily on steady-state results.

In many one-dimensional (1D) atom cooling experiments where an atomic beam traverses counterpropagating laser beams, steady-state solutions are not suitable for comparisons with experiment. For atoms that have been precooled in a 3D magneto-optic trap, the interaction times in a 1D standing wave may indeed be adequate to achieve steady state [10]. However, in experiments with a thermal atomic beam, the interaction time is typically no more than 1000τ to 2000τ, where τ is the excited-state radiative lifetime. The steady-state limit may not be attained, particularly when the initial velocity distribution is appreciably wider than the so-called capture velocity v_c. The range of atom velocities that are effectively slowed depends on the interaction time. Clearly, theoretical results for finite interactions times are of interest.

It will be demonstrated in this Rapid Communication that density-matrix methods over a basis of free-particle states or of eigenfunctions of the light-shift potential are capable of significant extension beyond their use as previously reported [3,4]. By efficient programing and the use of supercomputer technology, results have been obtained for the temporal evolution and for higher angular momentum. The computational techniques will be illustrated by both lin $\perp$ lin polarization gradient cooling (two counterpropagating laser beams with orthogonal linear polarizations) and magnetically induced laser cooling (MILC). Results will be shown for cases in which the incremental velocity change (the recoil velocity) is not small compared with the width of the velocity distribution, thus where semiclassical Fokker-Planck approaches would not be valid. Quantum methods will also be applied to atoms whose kinetic energy is less than the amplitude of the periodic light-shift potential. In this regime, the use of a constant velocity parameter in the computation of the semiclassical force function is inappropriate.

Calculations with a free-particle basis here include the excited state explicitly [3]. The basis states, $|F, m_F, n> = |F, m_F> \exp(inkz/\hbar)$, where $2\pi/k$ is the laser wavelength, are products of internal atomic sublevels and free-particle momentum eigenfunctions. In the evolution equation for the density matrix, $\dot{\sigma} = -(i/\hbar)[H, \sigma] + \dot{\sigma}_{\rm rel}$, the Hamiltonian H includes the laser-atom interactions (H_L) and possibly magnetic-field effects, while $\dot{\sigma}_{\rm rel}$ expresses the effects of spontaneous decay and repopulation, including an average over the spatial distribution of emitted light. Elements of H_L include photon recoil explicitly. Elements of σ are placed in a column vector x, and the coupled equations $\dot{x} = Wx$ are integrated numerically. These computer programs have been modified [11] to deal with transitions with $\Delta F = -1$ and 0, more than one ground- and excited-state hyperfine level, and spatially nonuniform laser intensity. In this report, however, only $F \rightarrow F + 1$ transitions are considered and the laser intensity is constant over the interaction region.

A full density matrix for up to ± 50 recoil momenta, even for a mesh spacing of one recoil and a $J = 1/2 \rightarrow 3/2$ transition, would have more than 3×10^4 elements and the evolution matrix would then have 10^9 elements. However, off-diagonal elements with $\Delta n > n_{\rm max}$ are found not to affect the computed velocity distribution. $n_{\rm max}$ varies with laser intensity and detuning but is typically 6 to 12. Effectively, σ becomes a band matrix of order n. In the present calculations, there were up to 100 000 density-matrix elements. The evolution matrix W can be simplified by neglecting elements less than 10^{-12} in magnitude, for example. No more than 20 to 50 elements are needed in each row for the free-particle basis approach. By such means, it is possible to compute the temporal evolution to 1000 radiative lifetimes with a basis of 65 momentum values for each (F, m_F) sublevel

in an $F = 3 \rightarrow 4$ transition with about 2 h of equivalent Cray XMP CPU time.

When the atoms are weakly excited, excited-state elements may be eliminated from the density-matrix equations to obtain a periodic light-shift potential for the ground state [4]. This approach gives a useful physical picture, and for certain applications, uses less computer time. The energy spectrum exhibits a band structure resembling that obtained for electron waves in a 1D crystal lattice. Optical pumping, magnetic-field mixing, and spontaneous emission rates are computed for density-matrix elements over the basis set of Bloch states.

Results obtained for the lin $\perp$ lin laser configuration, in which two counterpropagating laser beams have orthogonal linear polarization, show that the steady-state limit may not reliably represent cooling processes occurring over shorter interaction times. Figure 1 shows typical time evolution plots obtained with the free-particle basis. Here, $\varepsilon = E_R/\hbar\Gamma = 6.4 \times 10^{-4}$, as for Rb, where $E_R = \hbar^2k^2/2M = Mv_R^2/2$ is the recoil energy and Γ is the radiative decay rate. The laser field is characterized by the light-shift well depth, $U_0 = -fS\hbar\delta/L$. For lin $\perp$ lin cooling on an $F \rightarrow F+1$ transition, $f = [(2F+1)(F+1)-1]/[(2F+1)(F+1)]$, $S = 2\Omega^2/\Gamma^2$, where Ω is the single-beam Rabi frequency, $\delta = \omega_{\text{laser}} - \omega_{\text{atom}}$ is the detuning, and $L = 1 + 4\delta^2/\Gamma^2$. ($S = 1$ for laser intensity $I = hc/\lambda^3\tau$.) The calculations shown in Fig. 1(a), for $F = 1/2 \rightarrow 3/2$, are carried to 100 μs, or 3770τ, where $\tau = 1/\Gamma$. Ultimately, the velocity distribution $P(v)$ does evolve into the typical form for the asymptotic limit, namely a narrow Gaussian on top of a broad Gaussian [3] . However, up to 40 μs, the narrow Gaussian is flanked by two dips at the capture velocity, v_C (about $16v_R$ here).

With lower laser intensity or wider initial distribution over v, the dips at $v = \pm v_C$ persist for longer times. The generic behavior is shown in Fig. 1(b), for $F = 3 \rightarrow 4$. To extract an average kinetic energy for atoms in the central peak, two procedures have been used. The first assumes that the distribution for $|v| < v_C$ is Gaussian. The velocity $v_{1/e}$ at 1/e of the maximum height difference then yields a Gaussian average energy $E_{KG} = Mv_{1/e}^2/4 = (v_{1/e}/v_R)^2E_R/2$. In the second method, one computes the average kinetic energy E_{KA} of atoms in the range $|v| < v_C$. If the distribution in the central peak were truly Gaussian, $E_{KA} = E_{KG}$, but typically, $E_{KA} \sim 0.7E_{KG}$ (the Gaussian distribution extends beyond the dips at $v = \pm v_c$).

The variation of E_{KG} with laser parameters after 30 μs ($1{,}130\tau$ for Rb) is shown in Figs. 2(a) and 2(b). For the calculations shown in Fig. 2, $\varepsilon = 6.4 \times 10^{-4}$, $\delta = -5\Gamma$, and again the free-particle basis was used. To emphasize the role of the well depth, in Fig. 2(a) E_{KG}/U_0 is plotted vs U_0/E_R. For $F_g = 3$, the average kinetic energy (KE) in the cold-atom peak is significantly less than for $F_g = 1/2$. Since this trend seems to persist to longer interaction times, this may in part explain the experimental observation that the fraction of atoms in the lowest quantum state in experiments on ^{85}Rb, with $F_g = 3$, was larger than computed for $F_g = 1/2$ [10]. One possible explanation for the lower kinetic energies with high F_g is the greater importance of $\Delta m_F = \pm 2$ coherences induced by the laser field, which produce progressively larger off-diagonal elements in the light-shift potential matrix. For high F, energy bands within the potential well are broadened, making the motion for $EK < U_0$ more nearly like that of free particles (see also Ref. [8]).

For finite interaction times and $U_0/E_R < 100$, the average KE for atoms in the central peak is significantly below the average KE for the entire distribution obtained from the steady-state results, for which the minimum was $EK \sim 5E_R$ [4]. For atoms in the central peak, the lowest values in Fig. 2(b) are actually close to the minimum KE of about E_R, determined by quantum effects not represented in Fig. 2(b), but discussed in a recent study based on quantum calculations and observations on metastable He atoms [12].

For MILC [13,14], the light-shift potential matrix is diagonal and sinusoidal, so the wave equation for each

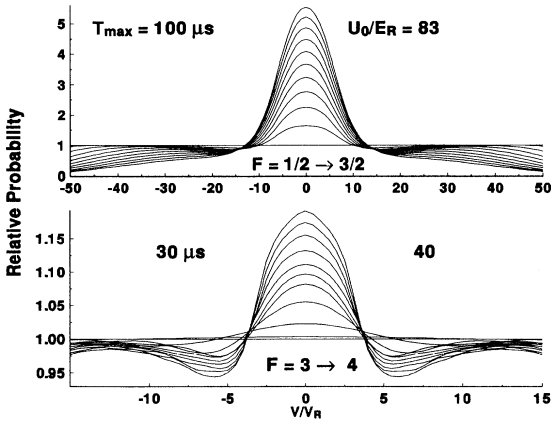

FIG. 1. Time evolution of lin $\perp$ lin laser cooling with Rb atoms ($\tau = 26.5$ ns). (Top) Detuning $= -\Gamma$, time interval between traces $= 10$ μs. (Bottom) Detuning $= -5\Gamma$, time interval $= 3$ μs.

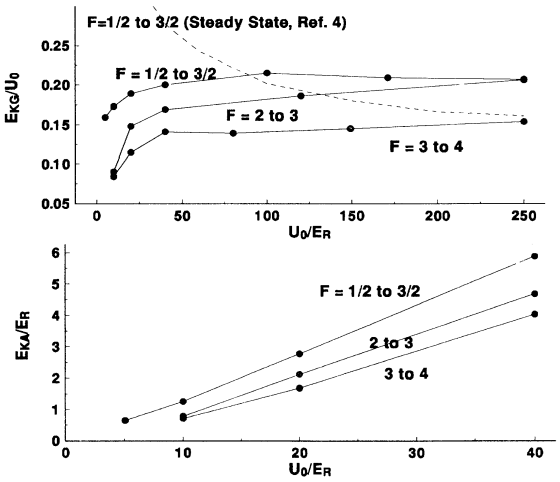

FIG. 2. Average kinetic energies after lin $\perp$ lin cooling of Rb atoms for 30 μs (1130τ). See text for definition of E_{KG}, E_{KA}, and U_0.

m_F is simply a Mathieu equation. The periodic potential basis approach is appropriate for $S/L \ll 1$. To model experiments in which atoms move freely outside the interaction region, an initially flat distribution over free-particle states is projected onto the periodic state basis. After computing the evolution to times t_i, the distribution over the periodic state basis is projected back onto the free-particle basis. $\mathrm{Tr}(\sigma)$ decreases by a few percent over typical interaction times because the total optical pumping rate out of any quantum basis state is greater than the repopulation terms from this level summed over any finite set of basis states. Results from the periodic potential basis states and free-particle basis states are very similar for weak excitation.

The temporal behavior computed for MILC exhibits a new feature associated with the localization of atoms in the standing wave. In MILC, the counterpropagating laser beams have identical circular polarization and the light-shift potential maxima and minima for different m_F sublevels are spatially in phase. A transverse magnetic field mixes different m_F sublevels, providing the same function as a polarization gradient. Zeeman mixing occurs most effectively at the nodes of the laser standing wave, where the potentials are degenerate. With red detuning, when the final kinetic energy is less than the depth of the light-shift potential wells in MILC, atoms in the ground state cannot traverse the potential peaks at the nodes, the magnetic-field mixing is suppressed, and the cooling rate slows. Although the asymptotic velocity distribution may still be nearly Gaussian, over very extended times there is a deficiency of the coldest atoms. The velocity distribution exhibits a flattened top, or even a minimum at $v = 0$. Figure 3 shows this effect in the velocity distribution for $F_g = 1/2$ [in Figs. 3(a)–3(c)] and for $F_g = 3$ [in Fig. 3(d)]. In MILC, the effective

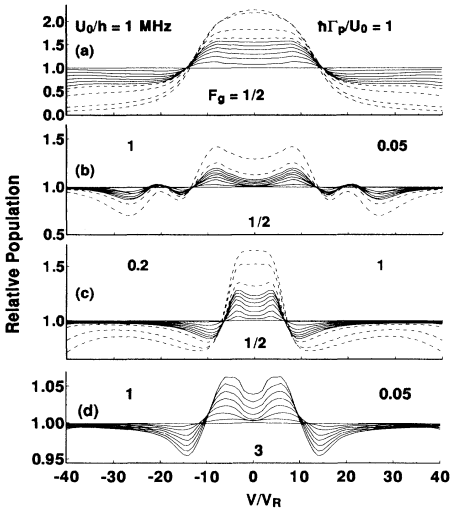

FIG. 3. Calculated free-particle velocity distributions with MILC for atoms with recoil energy 3.85 kHz, $\tau = 26.5$ ns (as for Rb) for interaction time intervals of 5 μs (solid lines) and 50 μs (dashed lines) for (a) $B = 5\mu$T, $S = 0.42$, $\delta = -\Gamma$; (b) $B = 5\mu$T, $S = 6.67$, $\delta = -20\Gamma$; (c) $B = 2\mu$T, $S = 0.083$, and $\delta = -\Gamma$; and (d) $B = 7.5$ μT, $S = 6.86$, $\delta = -20\Gamma$. The initial velocity distribution is flat to $\pm 50 V_R$.

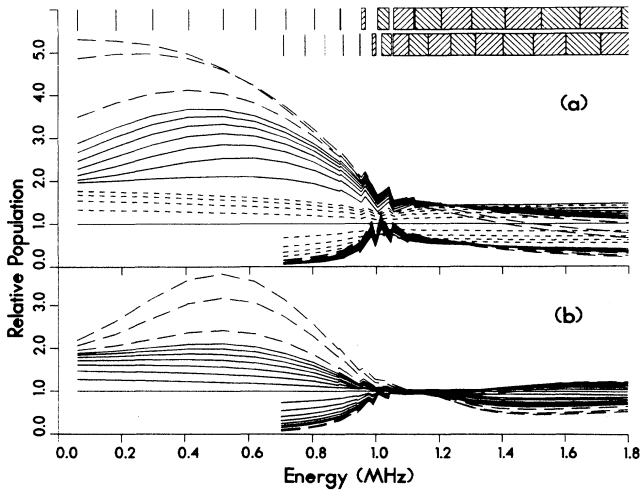

FIG. 4. Calculated populations of the eigenstates of the periodic light-shift potential for cases shown in Fig. 3(a) (top) and 3(b) (bottom). The well depth $U_0/h = 1$ MHz in each case. The time intervals are 0.3 μs (short dashed lines), 5 μs (solid lines), and 50 μs (long dashes). All levels initially have a population of 1 on this scale, and subsequently $m_F = 1/2$ levels become more populated, while $m_F = -1/2$ levels fall below 1. Band energies are displayed at the top. The distribution is non-Maxwellian for an extended time.

optical pumping rate, $\Gamma_p = 2S\Gamma/L$, and $U_0 = -2S\hbar\delta/L$. In Figs. 3(a) and 3(c), $\hbar\Gamma_p = U_0$. When $\hbar\Gamma_p$ is small compared with U_0, as in Figs. 3(b) and 3(d) for which $\hbar\Gamma_p = U_0/20$, the minimum in $P(v)$ at $v = 0$ is more persistent. Figures 4(a) and 4(b) show distributions over the

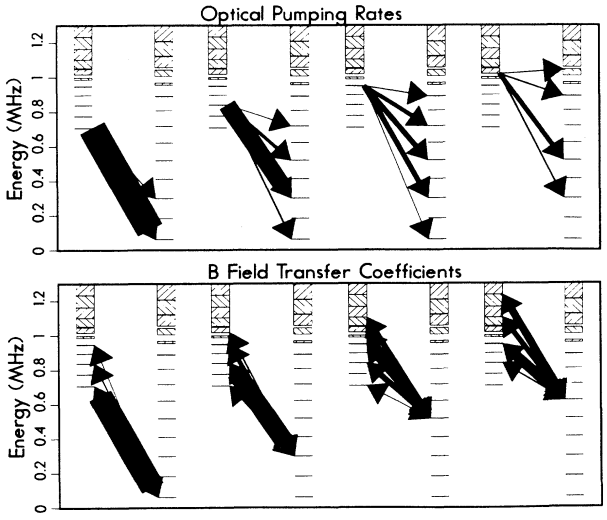

FIG. 5. B-field mixing coefficients and $\Delta m_F = 1$ optical pumping rates between quantum levels in the periodic light-shift potential, for an F = 1/2 → F = 3/2 σ^+ optical transition. Energy levels below the potential maxima (at 1 MHz in this case) and bands are shown for $m_F = -1/2$ (left in each transition pair) and for $m_F = 1/2$ (to the right in each pair). The width of each arrow is proportional to the magnitude of the mixing coefficient or the optical pumping rate.

states in the periodic potential corresponding to the $P(v)$ distributions shown in Figs. 3(a) and 3(b). The energies of these states are shown at the top of Fig. 4. Below the potential maxima, $U_0/h = 1$ MHz here, there are quasidiscrete states, while for $E > U_0$, the gaps between the bands are narrow. Although cooling increases the population of the states lying below U_0, the population of the lowest states increases very slowly, particularly when $\hbar\Gamma_p < U_0$.

For stationary states in the light-shift potential, the explanations for sub-Doppler laser cooling derived from semiclassical models [2] do not apply. A damping force does not explicitly enter the present calculations. In the quantum representation, cooling occurs because of preferential optical pumping out of higher-lying states into lower-lying states. The way this works in MILC is shown very schematically in Fig. 5 for states in the light-shift potential. Energy bands are shown in columns for $m_F = -1/2$ (left of each transition pair) and for $m_F = 1/2$ (right of each pair). The magnetic field and the laser interactions redistribute the populations over this basis set. The widths of the arrows indicate the relative optical pumping rates or B-field mixing coefficients. Not shown is the much slower process of diffusive heating in $\Delta m_F = 0$ excitation and decay. In the optical pumping process, on average the emitted photon takes away more energy than is added by the absorbed laser photon. This is due in part to the difference in the $m_F = \pm 1/2$ potential minima. In addition, optical pumping favors final states localized at the antinodes, namely the lower-lying states for red detuning. On the other hand, the magnetic field does not vary spatially over the interaction region, so the redistribution by the magnetic field is not so sharply peaked at $\Delta n = 0$. These processes constitute a cooling cycle. The reduction of energy in the $\Delta m_F = 1$ optical pumping part of the cycle is greater than the increase of energy that occurs in $\Delta m_F = -1$ magnetic-field mixing and in $\Delta m_F = 0$ diffusive heating.

Comparisons of the results present above with experiment are obviously of great interest. From preliminary results [15], it appears that the lin $\perp$ lin results are in good agreement with experiment on Rb and also that results for MILC agree well with experiments on He $2\,^3S$ [12]. However, experimental cooling peaks observed for certain MILC experiments with Rb [15] are narrower, without the dip at $v = 0$ found above. One possible explanation is that the optical wave fronts in the apparatus used for Rb are not ideal, and trapping in the light-shift wells occurs less than in the calculations. These comparisons and comparisons with semiclassical calculations will be discussed in future presentations.

This work was supported by NSF, ONR, and AFOSR. I am indebted to H. Metcalf, J. Dalibard, R. Gupta, E. Vredenbregt, M. Doery, and other colleagues for valuable discussions. Computing time was provided by the Cornell National Supercomputing Facility, which is funded by NSF and IBM.

[1] V. Minogin and V. Letokhov, *Laser Light Pressure on Atoms* (Gordon and Breach, New York, 1986).
[2] G. Nienhuis, P. van der Straten, and S.-Q. Shang, Phys. Rev. A **44**, 462 (1991).
[3] Y. Castin, J. Dalibard, and C. Cohen-Tannoudji, in *Light Induced Kinetic Effects on Atoms, Ions and Molecules*, edited by L. Moi *et al.* (ETS Editrice, Pisa, 1991).
[4] Y. Castin and J. Dalibard, Europhys. Lett. **14**, 761 (1991).
[5] K. Molmer *et al.*, J. Opt. Soc. Am. B **10**, 524 (1993).
[6] P. Marte, R. Dum, R. Taieb, and P. Zoller, Phys. Rev. A **47**, 1378 (1993).
[7] R. Taieb *et al.*, Phys. Rev. A **47**, 4986 (1993).
[8] P. Marte *et al.*, Phys. Rev. Lett. **71**, 1335 (1993).
[9] K. Berg-Sorensen *et al.*, Europhys. Lett. **22**, 663 (1993).
[10] P. Jessen *et al.*, Phys. Rev. Lett. **69**, 49 (1992).
[11] S. Padua *et al.*, Phys. Rev. Lett. **70**, 3217 (1993).
[12] M. Doery *et al.* (unpublished).
[13] P. Ungar *et al.*, J. Opt. Soc. Am. B **6**, 2072 (1989).
[14] B. Sheehy *et al.*, Phys. Rev. Lett. **64**, 858 (1990).
[15] S. Padua *et al.* (private communication).